KSCE Journal of Civil Engineering (2021) 25(1):78-91
DOI 10.1007/s12205-020-0508-1

pISSN 1226-7988, eISSN 1976-3808
www.springer.com/12205

Geotechnical Engineering

Factors Affecting Occurrence of Landslides Induced by the M7.8 April 2015, Nepal Earthquake

Rubini Mahalingam[a] **and Byungmin Kim**[b]

[a]*Ambiental Technical Solutions, Sussex Innovation Center, Falmer BN19SB, UK*
[b]*Member, School of Urban and Environmental Engineering, Ulsan National Institute of Science and Technology, Ulsan 44919, Korea*

ARTICLE HISTORY

Received 20 March 2020
Revised 22 June 2020
Accepted 14 August 2020
Published Online 11 November 2020

KEYWORDS

2015 Nepal earthquake
Landslide
Inventory
Statistical analysis

ABSTRACT

The **M**7.8 Nepal earthquake on 25 April 2015 and its aftershocks triggered thousands of landslides. Understanding correlations between the landslide occurrences and landslide conditioning factors is essential to generate a landslide susceptibility map. This study considers the two most reliable inventory data: landslide inventory 1 (LI-1) and landslide inventory 2 (LI-2). The LI-1 contains 1,352 landslide polygons, and the LI-2 contains 4,000 landslide points. The centroid locations of LI-1 were also considered as additional point inventory data for the statistical analyses. The landslide area percentage and landslide number density are computed for important factors such as slope angle, slope roughness, aspect, peak ground acceleration (PGA), distance to epicenter, distance to rivers and roads, Normalized Difference Vegetation Index (NDVI), land use and land cover, and mean annual precipitation. The cumulative percentage curves and the areas under the curve (AUC) are also compared for all the considered factors. PGAs of the main shock and two major aftershocks, distance to epicenter, slope angle, distance to river, and NDVI have relatively stronger correlations with the landslide occurrence than other factors. It is found that the LI-1 polygons have weaker correlations with the factors than LI-1 points and LI-2 points do because the LI-1 does not distinguish debris from scarps.

1. Introduction

Earthquakes in the Himalayan region dates back to about 160 million years when the Indian plate moved towards the northeast direction from the Antarctica plate and merged with Eurasian plate about 50 million years ago (Gupta, 2015). The Himalayan mountain range is the result of this collision (Bilham et al., 1997). Several authors studied the movement of this plate and found out that the Indian plate is moving with a velocity of ~5 – 6 cm/year and a portion of this convergence movement is built up in the Himalayan range (e.g., Yeats and Lillie, 1991; Bilham et al., 1997; Jade et al., 2004). The strains built up in the continental collision plate boundary is released in frequent earthquakes. Historical investigations indicate that the largest earthquake in Himalayan region was on August 15, 1950, with a moment magnitude (**M**) of 8.7 (e.g., Murty and Rafiq, 1991; Ambraseys and Bilham, 2000; Gahalaut and Kundu, 2012). Richter et al. (1958) documented the history earthquakes in the Indian region. Major devastating earthquakes occurred in Nepal and the central Himalayas are summarized in Bilham et al. (1995), Bilham and Ambraseys (2005), and Pandey and Molnar (1988). Disaster Preparedness Network has a published record of historical earthquakes in Nepal dating from 1255 AD (http://www.dpnet.org.np/index.php?pageName=earthquake).

Due to this active tectonic setting, Nepal has experienced numerous seismically induced landslides (e.g., Dahal and Hasegawa, 2008) which pose a great threat to public safety. An average loss of 100 people in a period of 5 years due to landslide activities, was reported by the Nepal government (Nepal Disaster Risk Reduction Portal) (http://drrportal.gov.np/.). The recent **M**7.8 earthquake on April 25, 2015 and its aftershocks killed more than 8,000 people and incurred a loss of about 4 billion USD (USGS) (http://earthquake.usgs.gov/learn/topics/Nepal_Slides.pdf) and triggered thousands of landslides. Fig. 1 shows landslide observations from the pictures that one of the authors took around Kathmandu and Gorkha, Nepal in May 2015. Therefore,

CORRESPONDENCE Byungmin Kim byungmin.kim@unist.ac.kr School of Urban and Environmental Engineering, Ulsan National Institute of Science and Technology, Ulsan 44919, Korea

© 2021 Korean Society of Civil Engineers

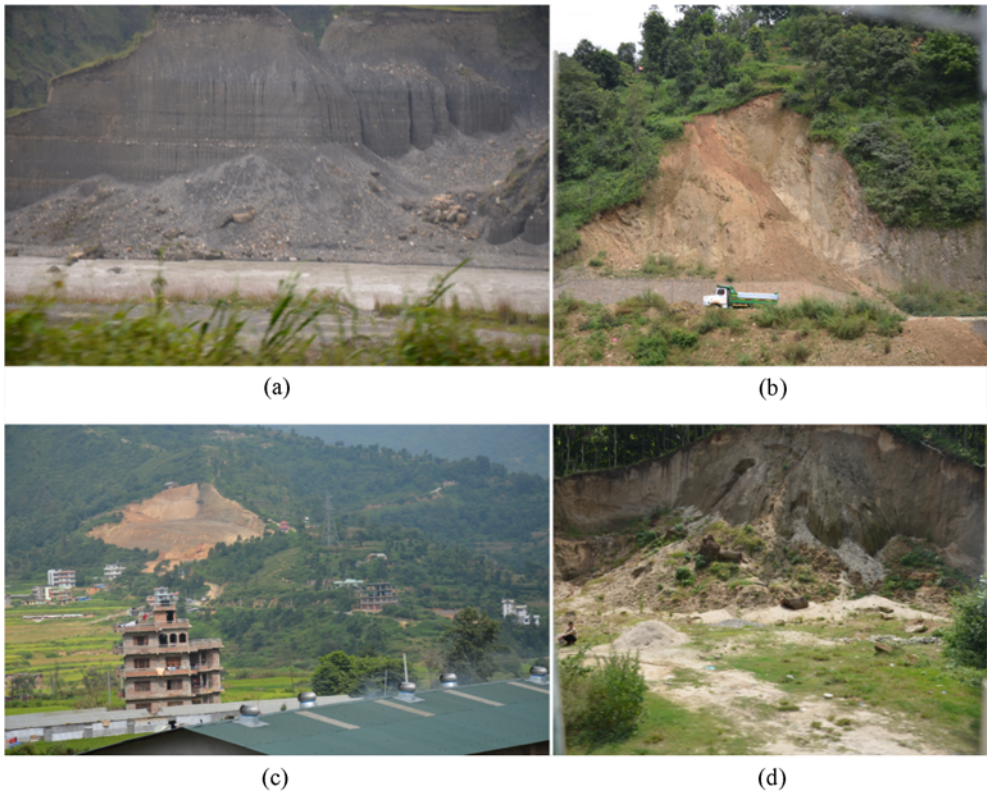

Fig. 1. Examples of Landslides Caused by the 2015 Nepal Earthquake: (a) Landslides on the Bank of the Bagmati River (27.403°*N*, 85.447°*E*), (b) Landslides on the Shoulders of the National Highway (H04), Connecting Kathmandu and Pokhara, Nepal (27.986°*N*, 84.298°*E*), (c) Landslides in the Natural Herbaceous and Low Shrubs area near Salang Ghat (27.806°*N*, 84.894°*E*), (d) Landslides in the Needle Leaved Plantation Area near the Village Charaundi (27.798°*N*, 84.738°*E*) (The coordinates indicate the locations where the pictures were taken.)

it is important to develop a landslide susceptibility map for risk assessment and mitigation efforts for Nepal to minimize human and economic losses during such natural hazards.

Thousands of landslides which occurred during the **M**7.8 April 25, 2015 earthquake and its aftershocks in Nepal were thoroughly identified by multiple sources by means of satellite images and field investigations. This study considers two distinct inventory data sets in different formats (i.e., polygons and points) compiled in different time periods (i.e., immediately after the earthquake and several months later) to examined the effects of conditioning factors in triggering landslides. This study also considers various hazard factors such as peak ground acceleration (PGA) and epicentral distance, as well as various vulnerability factors to the slope such as slope geometry, geology, land cover, vegetation index, precipitation, and distances to river and road. The results of this study can be used as an important segment in developing a seismically induced landslide susceptibility map for Nepal.

2. Seismic Landslides Triggered during the 2015, M 7.8 Nepal Earthquake and Its Aftershocks

A statistical analysis of the landslide distribution with respect to triggering factors requires a significant collection of the latest and accurate data sets. Satellite remote sensing techniques are widely used for rapid landslide detections. The British Geological survey, Durham University, International Centre for Integrated Mountain Development (ICIMOD), Mississippi Disaster Recovery (MDA), and National Geospatial-Intelligence Agency (NGA) identified the landslide locations and published them through the International Charter Disaster Activation (ICDA), in its report 530/531 (National Environment Research Council) (https://www.bgs.ac.uk/research/earthHazards/epom/documents/LandslideinventoryNepal). These agencies acquired images before and after the earthquake from Worldview, DMCii (DMC International Imaging), SPOT (Satellite Pour l'Observation de la Terre), Pleiades, and Radarsat satellites to identify the landslide locations. The Geotechnical Extreme Event Reconnaissance (GEER) reported the landslide locations based on their field investigation (Hashash et al., 2015). The five landslides polygons based on the coordinates mentioned in the report were appended to the inventory provided by ICDA. There were no spatial intersections of the polygons produced by ICDA and GEER. This study compiled the landslide inventory data from these sources in a polygon format and named as landslide inventory 1 (LI-1). In addition to the areal locations of landslides, the centroid point for each of the landslides is considered in the subsequent analyses.

The ICIMOD released landslide location points compiled by the Volunteer Group [organized by University of Arizona and supported by the Global Land Ice Measurements from Space (GLIMS)] who used the satellite images from the NASA,

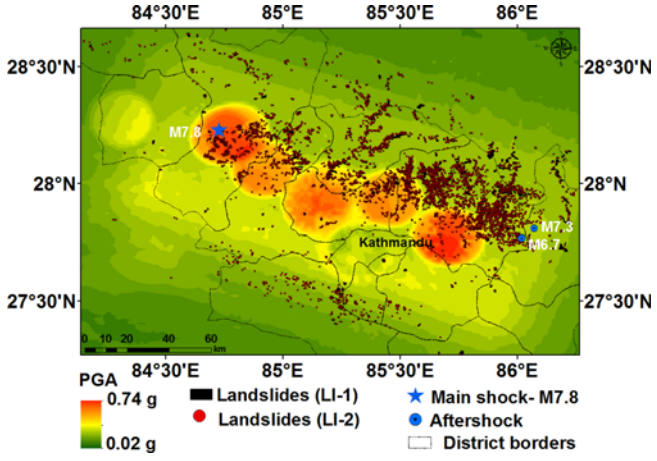

Fig. 2. Spatial Distribution of Landslides Generated during the **M**7.8 Nepal Earthquake and Its Aftershocks (**M**7.3 and **M**6.7) Overlaid on a PGA Map of the Main Shock (USGS ShakeMap) (Landslides (LI-1) – inventory obtained by digitizing published maps/ reports published by ICDA. Landslides (LI-2) – inventory generated by ICIMOD and obtained from Kargel et al. (2016))

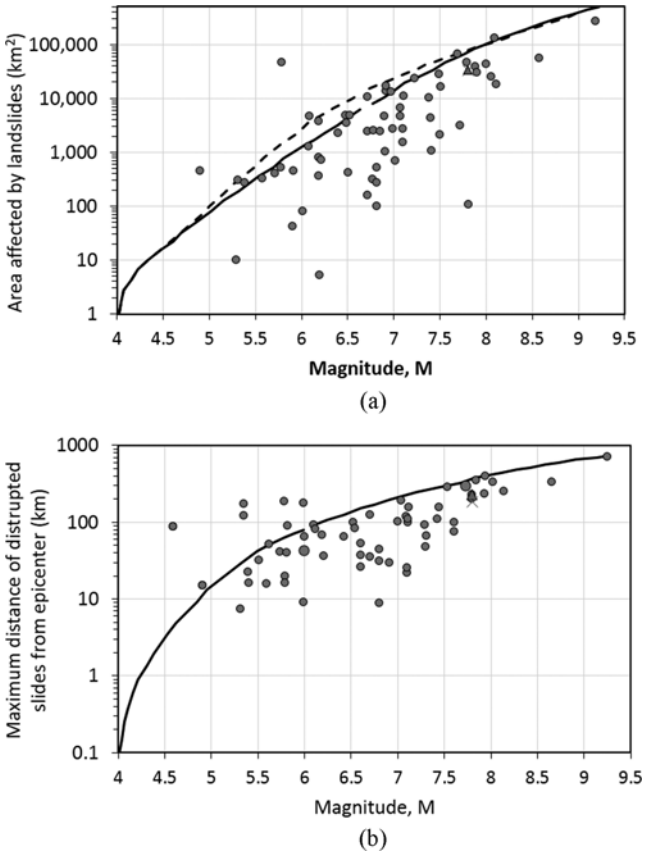

Fig. 3. Landslide Area and Maximum Distance: (a) Area Affected by Landslides versus Earthquake Moment Magnitude, (b) Maximum Distance of Landslides from the Epicenter versus Moment Magnitude (The solid line is an upper bound by Keefer (1984) and dashed line is an upper bound by Rodríguez et al. (1999). Cross symbol and triangle symbol represent the values from two inventories (LI-1 and LI-2, respectively) for the Nepal earthquake on April 25, 2015. The grey circles denote data for other major earthquakes across the globe (Keefer, 1984; Rodrıguez et al., 1999; Jibson et al., 2004; Dai et al., 2011))

DigitalGlobe, Japan Aerospace Exploration Agency (JAXA), Planet Labs, SPOT images, MacDonald Dettwiler and Associates (MDA), and China National Space Administration (Kargel et al., 2015). This inventory data (LI-2) were used separately from the LI-1.

The LI-1 includes 1,352 landslide polygons measuring a total area of 924 km^2 extending to 14 Nepal districts as shown in Fig. 2. The LI-2 includes 4,000 point features mapped from high-resolution aerial imageries with spatial resolutions ranging between 1 m to 30 m. The LI-1 was available within the first few weeks of the earthquake, whereas the LI-2 was generated several months after the earthquake with extensive mapping tools and expert involvement. The repetitive landslides were removed by the agencies who released the inventory data. It was manually checked that all the LI-1 landslides are included in the LI-2. There are some landslides occurred in India and Nepal. However, those occurred within Nepal (the 14 districts) were used in the subsequent analyses.

With the recent advancements in remote sensing techniques, rapid landslide assessment is employed within the first few days of the earthquake events to map the landslide locations. This rapid landslide assessment produces point data. The polygon data are acquired later and provide more detailed information about the inherent characteristics of landslides and its locations. However, the polygon data may not differentiate landslide debris from scarps, resulting in uncertainty regarding the actual locations where the landslides are initiated. On the other hand, the point data may better represent the locations of initiation. Because of these advantages and disadvantages of point and polygon data, the both data types are considered in this study.

Figure 3(a) shows an approximate area of the extent of landslides triggered by the 2015 Nepal earthquake compared with those by worldwide historical earthquakes (Jibson et al., 2004). The area of landslide extent calculated from the LI-1 approximately 33,444 km^2, and from the LI-2 is 33,549 km^2, which are just below the upper bounds developed by Keefer (1984) and Rodrıguez et al. (1999) from worldwide historical earthquake data. Similarly, the maximum epicentral distance of landslide occurrences from historical earthquake data versus magnitude is shown in Fig. 3(b). The farthest distance of landslide distribution from the epicenter of the 2015 Nepal earthquake computed from the LI-1 and LI-2 are approximately 185 km and 230 km, respectively. Both the epicentral distances are just below the upper bound developed by Keefer (1984) from the worldwide historical earthquake data.

3. Spatial Correlations of Landslides with Conditioning Factors

Multivariate and bivariate analyses are widely used statistical methods for landslide correlation analyses (e.g., Nandi and Shakoor, 2010; Wang et al., 2016a; Wang et al., 2016b; Chu et

al., 2019). The multivariate method uses a higher degree of prediction which involves landslide inventory and its relationship with landslide conditioning factors. In the case of the bivariate analysis, the influence of each variable is tested independently on the landslide inventory for its correlation strength (Nandi and Shakoor, 2010). Although the multivariate analysis is proven relatively advanced than the bivariate analysis, the latter is proven effective for regional level analysis (Thiery et al., 2007; Arabameri et al., 2019). In addition, the bivariate analysis has been proven robust and effective in understanding the correlation values and to produce landslide susceptibility maps when limited information is available about the landslide inventory (Thiery et al., 2007). Given the fact that the landslide inventory and other data are still in a preliminary quality and require further improvement, the bivariate analysis is employed in this study to understand the spatial correlation of landslides and its conditioning factors. Improving the existing inventory is beyond the scope of this study. This study focuses on evaluating controlling factors using the best available landslide inventory.

Xu et al. (2013) used two indices to study the correlation of landslides triggered in Wenchuan earthquake, China. Similar indices are used in this study, namely the landslide area percentage (LAP) and landslide number density (LND). The LAP is described as an area affected by landslides per square kilometers. The LND is defined as a number of landslides per square kilometers. The LI-1 was used to derive LAP and LND values, and LI-2 was used to derive LND values for the landslide conditioning factors.

Conditioning factors were selected based on several previous studies (Chen et al., 2011). The selected parameters include seismic parameters of main shock with **M**7.8, aftershocks with **M**7.3 and **M**6.7 (i.e., peak ground acceleration (PGA), and

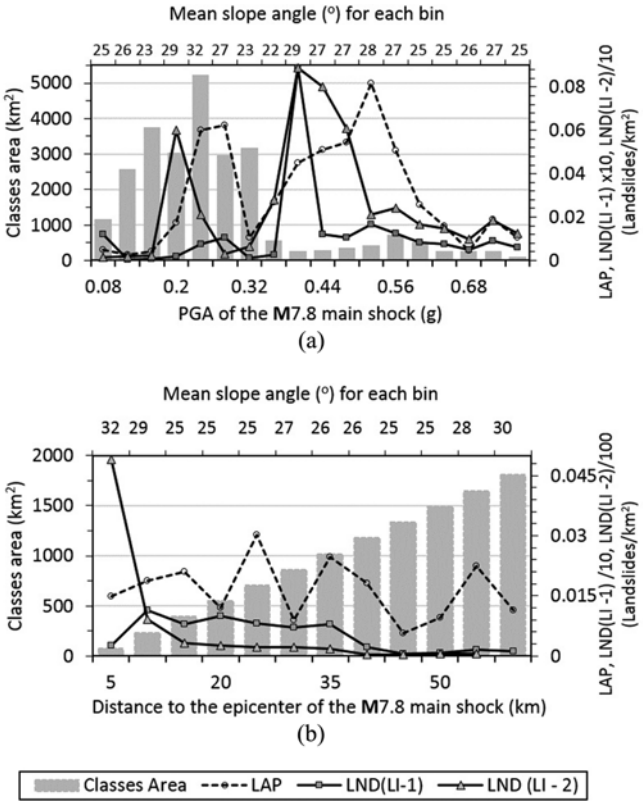

Fig. 4. Class Area, Landslide Area Percentage (LAP (LI-1)), and Landslide Number Density (LND (LI-1)), LND (LI-2) for Seismic Parameters: (a) Peak Ground Acceleration (PGA) from the **M**7.8 Main Shock Earthquake Event, (b) Distance to the Epicenter of the **M**7.8 Main Shock Earthquake (The numbers at the top of each panel represent mean slope angle values for parameter bins.)

Table 1. Landslide Conditioning Factors and Its Sources

Name	Source	Resolution/scale	Range
Landslide inventory (LI-1)	International Charter Disaster Activation	1:5,000 (maps) and 2.5 m to 22.5 m (satellite images)	Min: 0.01 km^2 Max:20.79 km^2 Mean:0.68 km^2 Std. dev. 1.51km^2
Landslide inventory (LI-2)	International Centre for Integrated Mountain Development (ICIMOD)	2.5 m to 22.5 m (satellite images)	Not applicable since it is a point inventory
Elevation	Shuttle Radar Topography Mission	90 m	0 – 8069 (m)
Slope, aspect, and slope roughness	Elevation model	90 m	Slope : 0 – 87°; Aspect : 0 – 360°; Slope roughness: 0 – 44°
Road	DIVAGIS	1:750,000	--
River	DIVAGIS	1:750,000	--
Mean annual precipitation	WorldClim	500 500 m	30 - 4050 mm/year
Geology	USGS	1:10,000,000	--
PGA	USGS ShakeMap	1:250,000	--
LULC	Food and agriculture organization of the United Nation	1:350,000	--
NDVI	USGS	30 × 30 m	-0.6 – 0.8

distance to the epicenter), topographical parameters (i.e., slope angle, slope roughness, aspect), geology, land use and land cover (LULC), Normalized Difference Vegetation Index (NDVI), distance to rivers, distance to roads, and mean annual precipitation. The maps for these parameters are shown in Figs. 2 and 11 through Fig. 13 (in Appendix), along with the landslide locations from LI-1. However, both the LI-1, and LI-2 are used for the analysis in this study. The sources and resolutions of these parameters are summarized in Table 1. The slope angle is considered to have the strongest influence on the occurrence of natural landslides (i.e., gravity-induced). Therefore, the influence of slope angle is considered in combination with other parameters.

3.1 Correlations with Seismic Parameters

Figure 4(a) shows the LAP (using the LI-1), LND (LI-1), and LND (LI-2) for PGA bins, as well as the area of each PGA bin. The LAP (LI-1) and LND (LI-1) increase with the PGA until the PGA of 0.3 g beyond which they do not show clear trends. The LAP (LI-1) shows bimodality with two peaks at PGAs of approximately 0.28 g and 0.52 g, and the LNDs (from both LI-1 and LI-2) are highest at PGA of 0.4 g. The small LAP (LI-1), LND (LI-1), and LND (LI-2) values at PGA bins between 0.32 g and 0.36 could be due to gentle slopes compared to other PGA bins as indicated in mean slope angle values at the top of the plot. This observation indicates that the influence of other factors like a slope angle might be stronger than that of the PGA. The LAP and LND values for PGAs larger than 0.56 g are small, unlike the intuition. This could be because the slopes are gentler for those bins.

High landslide density is witnessed near the epicenters of two aftershocks (with magnitudes of 6.7 and 7.3 occurred on April 26, 2015 and May 12, 2015, respectively) as shown in Fig. 2. Fig. 4(b) shows the LAP and LND values for the distance to the epicenter of the **M**7.8 main shock earthquake event. The LAP (LI-1) does not show a clear trend with the distance to the epicenter. The LND (LI-1) increases as the epicentral distance decreases until the distance of 10 km. At epicentral distances shorter than 10 km, the LND (LI-1) decreases with decreasing epicentral distance. However, the LND (LI-2) shows a strong correlation with the distance and is largest at the shortest distance for which the mean slope angle is also largest.

3.2 Correlations with Topographical Parameters

An elevation model is considered as the primary component for landslide analysis (e.g., Wei et al., 2014; Kadirhodjaev et al., 2018; Lee et al., 2018). The Shuttle Radar Topography Mission (SRTM) elevation data released in 2014 was used to generate the elevation data for Nepal. Topographical factors such slope angle, aspect, and slope roughness were derived from the elevation data as shown in the appendix (Fig. 11). These factors are commonly derived from elevation datasets and represent the characteristics of landslides for further analysis (Mahalingam et al., 2016). The class areas, LAP (LI-1), LND (LI-1), and LND (LI-2) for slope, slope roughness, and aspect are shown in Fig. 5.

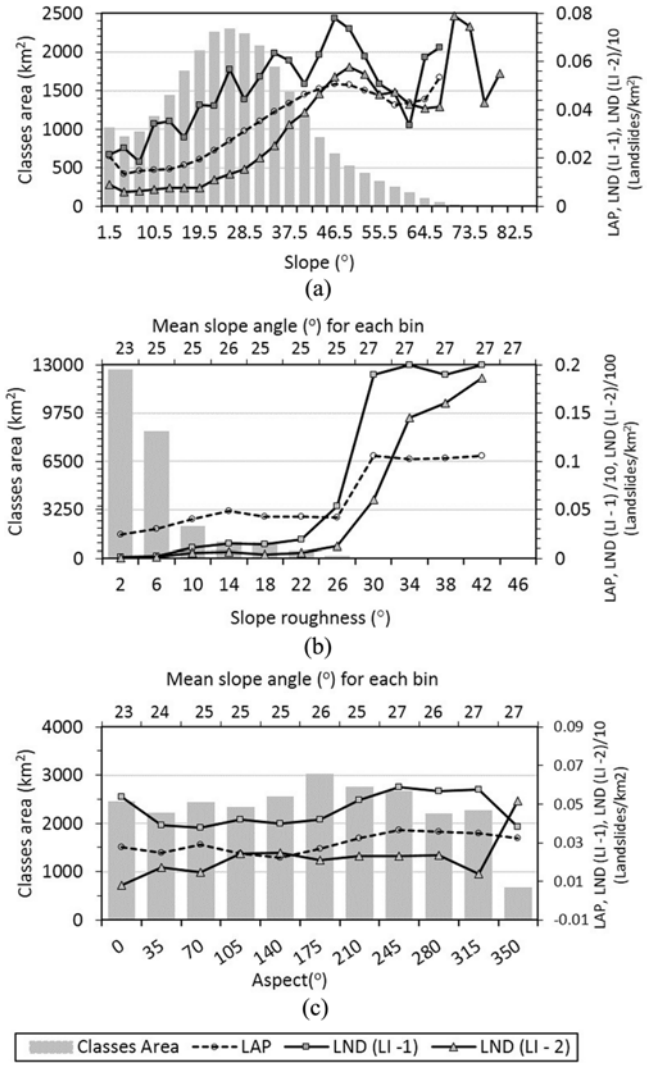

Fig. 5. Class Area, Landslide Area Percentage (LAP (LI-1)), and Landslide Number Density (LND (LI-1)) and LND (LI-2) for Topographic Parameters: (a) Slope, (b) Slope Roughness, (c) Aspect (The numbers at the top of each panel represent mean slope angle values for parameter bins.)

The slope angle is a significant factor for landslide occurrence even without a trigger, and steeper slope angles are highly susceptible to slope failures. The slope angle is derived from elevation grids (90 × 90 m) from the SRTM data, and ranges from 0 to 87° as shown in the appendix (Fig. 11(a)). The slope map was then reclassified into 3-degree intervals. The LAP (LI-1) and LNDs are also classified in the same intervals as shown in Fig. 5(a). The LAP (LI-1), LND (LI-1), and LND (LI-2) values generally increase with slope angle, indicating higher landslide occurrences in steeper slopes. However, these do not show clear trends for slope angles greater than 40°. The slope roughness computed as the standard deviation of neighborhood pixels (3 × 3 pixels) from the slope map as shown in the appendix (Fig. 11(b)). This parameter is considered to be an important controlling factor for slope stability in rough terrains (Mahalingam et al., 2016).

The slope roughness is reclassified into 4 degree intervals as shown in Fig. 5(b), along with the LAP (LI-1), LND (LI-1), and LND (LI-2) distribution. The LAP (LI-1), LND (LI-1), and LND (LI-2) values gently increase with the slope roughness, and abruptly increase when the slope roughness is greater than 20°. The LAP (LI-1), LND (LI-1), and LND (LI-2) do not have a significant correlation with aspect values as shown in Fig. 5(c).

3.3 Correlations with Geology and Surface Parameters

It is well known that soil's shear strength is related to geology. Therefore, geology is an important factor for landslide occurrence, and different geologic units have different landslide susceptibility values (e.g., Kargel et al., 2015). In order to understand the correlation between landslide occurrence and geology, a geological map in the scale of 1:10,000,000 was obtained in a vector map format (USGS) (http://energy.usgs.gov/OilGas/AssessmentsData/WorldPetroleumAssessment/WorldGeologicMaps.aspx). Then, the vector format of geology is converted to a raster format to maintain the consistency of analysis. The geologic time scale for the study area is divided into 13 units as shown in Fig. 12(a). The LAP (LI-1), LND (LI-1), and LND (LI-2) for geologic time scale are shown in Fig. 6(a). The LAP and LNDs are high for Quaternary (Q) deposits and Tertiary igneous rocks (Ti), and are lowest for Mesozoic Intrusive (Mi) and Neogene (N) deposits where the mean slope angles are smaller than for other geologic deposits. The LAP and LNDs are exceptionally low for Cretaceous sedimentary rocks (Ks) despite the mean slope angle of 31°. The LAP and LNDs generally increase with the geologic time scale for Jurrasic metamorphic and sedimentary rocks (Jms) and older [i.e., Triassic metamorphic and sedimentary rocks (Trms); Upper Paleozoic (Pzu); Lower Paleozoic (Pzl); and Precambrian (pC)]. This could be because of that the older rocks underwent more weathering processes.

Several researches have indicated that step/terrace farming are conducive for landslides (e.g., Gerrard and Gardner, 2002; Sidle et al., 2006). Therefore, it was important to understand which land use type is susceptible to earthquake-triggered landslides in Nepal. A land use and land cover (LULC) map was obtained from an open source data provider (Food and agriculture organization of the United Nation) (http://www.fao.org/docrep/003/x0596e/x0596e00.HTM) in vector format in the scale of 1:350,000. The land use type was divided into 10 classes as shown in Fig. 12(b). The LAP (LI-1), LND (LI-1), and LND (LI-2) for land use type are shown in Fig. 6(b). The LAP (LI-1), LND (LI-1), and LND (LI-2) are higher in needle leaved plantation types (NL) and natural herbaceous and low shrubs (NH&LS). This can be explained by the spatial distribution of NL and NH&LS near the high PGA values in that study section as shown in Figs. 2 and 12(b), as well as the high mean slope angles for these two categories. Despite the high mean slope angle, the LAP and LNDs for the Snow and Ice (S&I) region are low because this region is located far from the earthquake source (see Figs. 2 and 12(b)). The bare area, urban area (UA), and near rivers and water bodies (NR) have small mean slope angles, therefore, have low LAP and LND values. Despite the moderate mean slope angle (24°), the broad leaved area (BL) has low LAP and LND values. This might demonstrate the effect of broad leaved vegetation in reducing landslide susceptibility. It is worth noting that the agriculture valley (Ag. valley) region experienced very few landslides because of the gentle slopes and it is relatively far from the epicenters of the **M**7.8 main shock earthquake and its aftershocks.

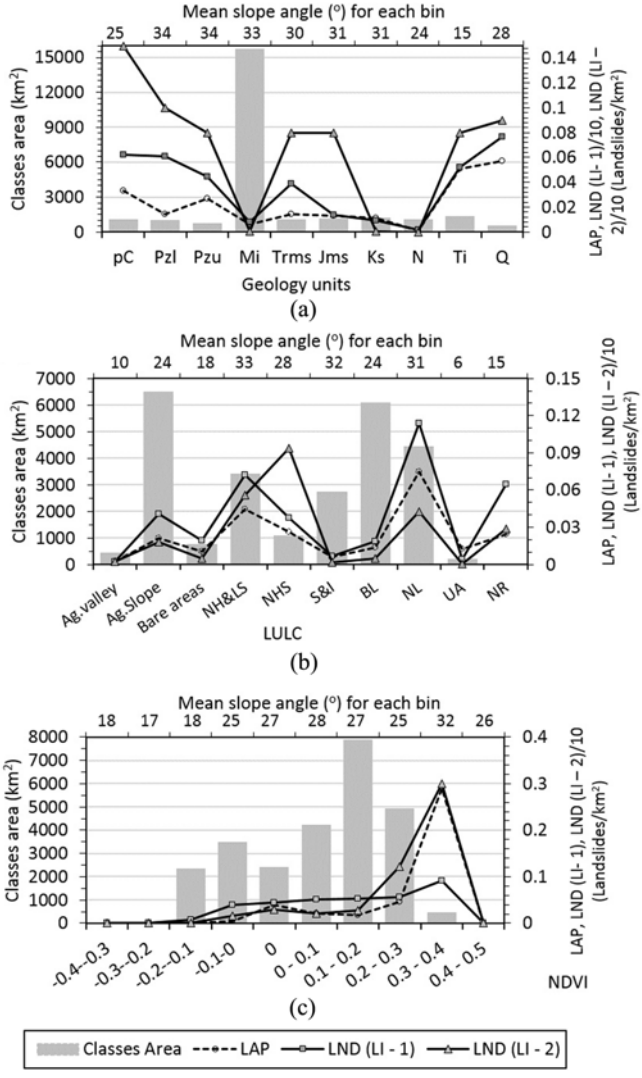

Fig. 6. Class Area, Landslide Area Percentage (LAP (LI-1)), and Landslide Number Density (LND (LI-1)) and LND (LI-2) for Surface Parameters: (a) Geology, (b) LULC, (c) NDVI (The numbers at the top of each panel represent mean slope angle values for parameter bins. Acronyms for geology are Precambrian (pC); Lower Paleozoic (Pzl); Upper Paleozoic (Pzu); Mesozoic Intrusive (Mi); Triassic metamorphic and sedimentary rocks (Trms); Jurrasic metamorphic and sedimentary rocks (Jms); Cretaceous sedimentary rocks (Ks); Tertiary igneous rocks (Ti); Neogene (N); Quaternary (Q). Acronyms for LULC are Natural herbaceous and low shrubs (NH&LS); Natural high shrubs (NHS); Snow and Ice (S&I); Broad leaved (BL); Needle leaved (NL); Urban areas (UA); Near river and water bodies (NR).)

NDVI is a vegetation index for photosynthetic activity and greenness of the area. The NDVI has been used in several studies to analyze the correlation of landslide occurrence (e.g., Lee and Dan, 2005; Lee and Pradhan, 2007). The NDVI is generated from red and near infra-red bands from the Landsat 8 (USGS) (https://landsat.usgs.gov/landsat-collections) with cloud cover less than 10%. In order to consider the vegetation as a landslide triggering factor, the NDVI acquired before April 25, 2015 was used. The NDVI ranges between -1 and 1, indicating no vegetation to complete vegetation, respectively. The grid was then reclassified with an interval of 0.1 to compute class distribution, LAP (LI-1), LND (LI-1), and LND (LI-2) as shown in Fig. 6(c). The mean slope angle increase with NDVI, which indicates more vegetation for steeper slope areas compared to gentle slope areas. The LAP and LNDs increase with an increase in NDVI values and are highest at a NDVI of 0.3 – 0.4 where the mean slope angle is also largest.

3.4 Correlations with Manmade and Hydrological Parameters

Undercutting effects of the river and cut slopes near the roads increase the magnitude of slope failures during the seismic activity (e.g., Liu et al., 2015). During the field visits around Kathmandu and Gorkha, Nepal in May 2015, the authors witnessed landslides near the roads and rivers as shown in Fig. 1 (a and b). Locations of rivers and roads were obtained from an open source data portal (divagis.com) and distances to rivers and roads were estimated as shown in Figs. 13(a) and 13(b). It is worth noting that clusters of landslides are found at short distances to rivers and roads.

The LAP (LI-1), LND (LI-1), and LND (LI-2) increase as the distance to rivers decreases as shown in Fig. 7(a). The LAP (LI-1) and LND values are higher within 3 km of rivers despite gentle slopes for these bins. This implies the strong influence of the distance to rivers on landslide occurrence. A slight increase in the LND value at a distance of 11 km is also attributed to its proximity to the epicenter of the aftershocks. The epicenter of the **M**7.3 aftershock is 2 km away from a part of buffer distance of 11 km around one of the rivers, and the epicenter of the **M**6.7 aftershock is within a buffer distance of 11 km around one of the rivers. Although the landslide inventory data used in this study do not differentiate landslides caused by the aftershocks and those by the main shock, it is of the authors' opinion that the aftershocks contributed to the landslide triggering. The statistical analyses for aftershock parameters in the next section supports this. The LAP (LI-1), LND (LI-1), and LND (LI-2) values in terms of distance to roads show similar trends with those for distance to rivers as shown in Fig. 7(b).

Annual precipitation is also an important landslide conditioning factor (e.g., Ray and Jacobs, 2007). The precipitation map was obtained from the major climate databases compiled by the Global Historical Climatology Network (GHCN), the FAO (Food and Agricultural organization of the United Nations), the WMO (World Meteorological Organization), the International

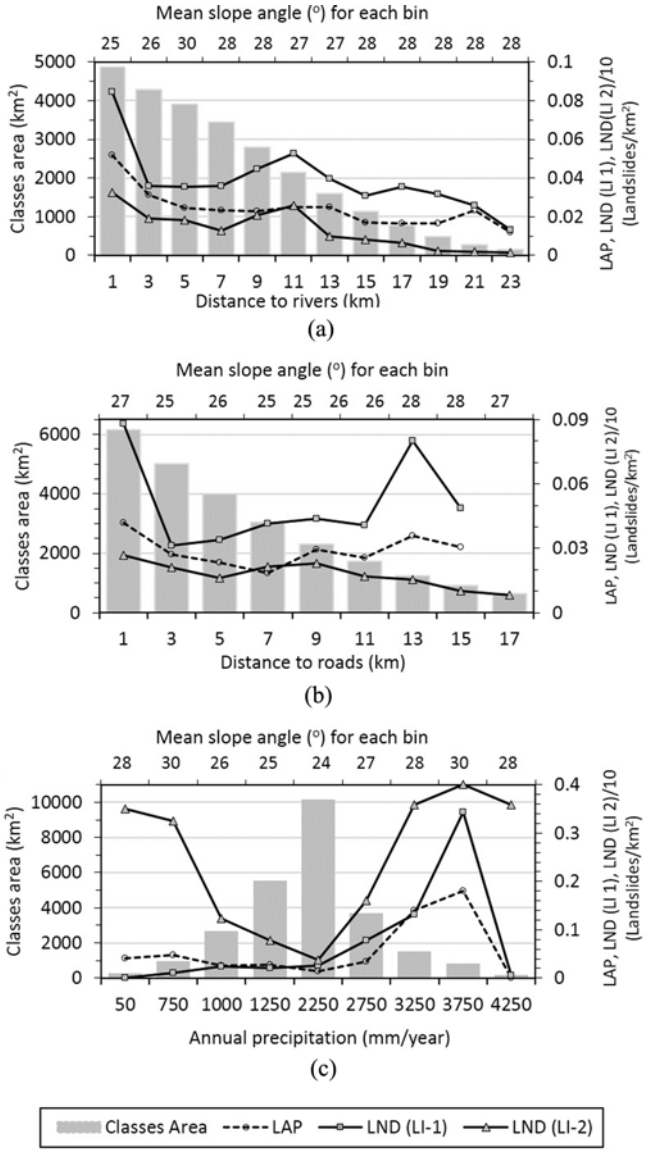

Fig. 7. Class Area, Landslide Area Percentage (LAP (LI-1)), and Landslide Number Density (LND (LI-1)) and LND (LI-2) for Categorical Parameters: (a) Distance to Rivers, (b) Distance to Roads, (c) Annual Precipitation (The numbers at the top of each panel represent mean slope angle values for parameter bins.)

Center for Tropical Agriculture (CIAT), R-HYdronet, and a number of additional minor databases for Australia, New Zealand, the Nordic European Countries, Ecuador, Peru, Bolivia, and from data published by Nepal government agencies (Department of Hydrology and Meteorology (http://www.dhm.gov.np/meteorological-station/). The data was made available through WorldClim (http://www.worldclim.org/version1) and is average precipitation over a time period of 1960 – 2000, which was spatially interpolated from stations on a 30 arc-second resolution grid. The best available data for precipitation for Nepal is available until 2000. The mean annual precipitation was verified with recent precipitation data measured at five stations (Government

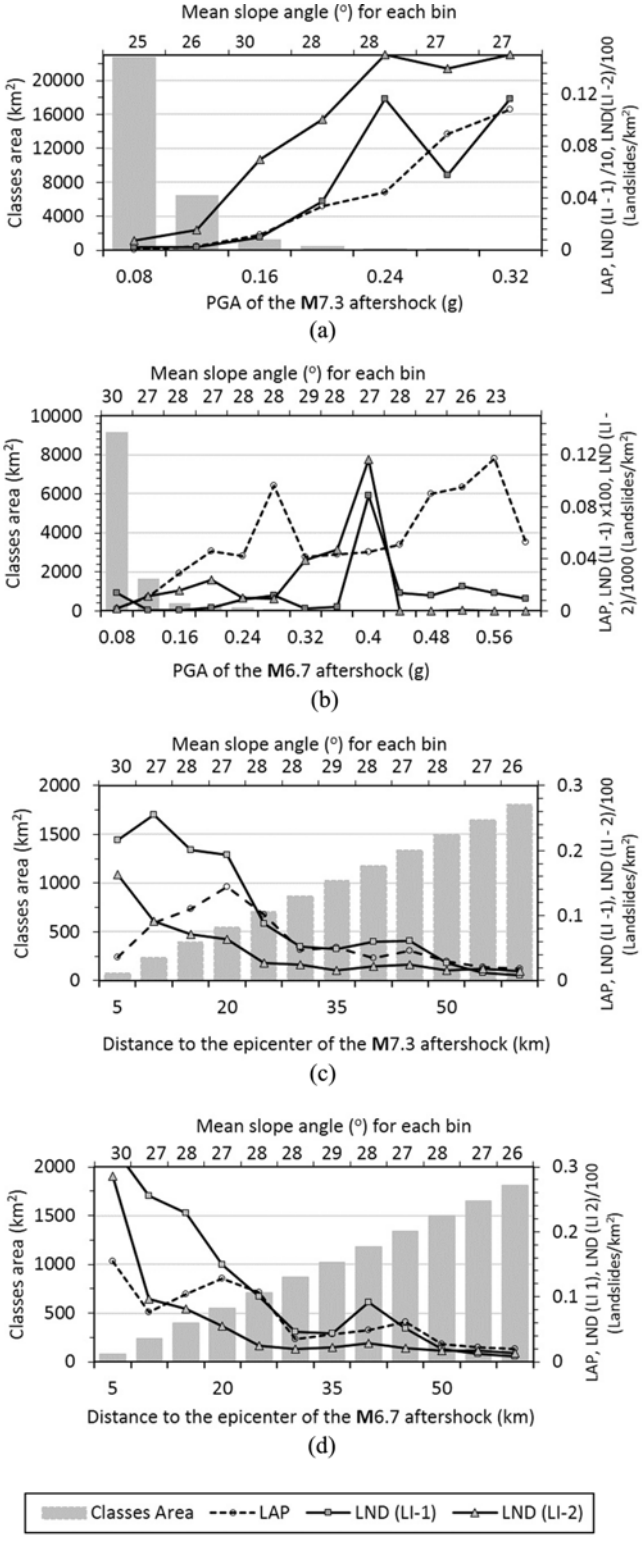

Fig. 8. Class Area, Landslide Area Percentage (LAP (LI-1)), and Landslide Number Density (LND (LI-1)), LND (LI-2) for Seismic Parameters: (a) Peak Ground Acceleration (PGA) from the Aftershock Event – **M**7.3 Earthquake, (b) Peak Ground Acceleration (PGA) from the Aftershock Event – **M**6.7 Earthquake, (c) Distance to Epicenter – **M**7.3 Earthquake, (d) Distance to Epicenter – **M**6.7 Earthquake (The numbers at the top of each panel represent mean slope angle values for parameter bins.)

of Nepal) (http://mfd.gov.np/report/?timeOfDay=0&date=2015-05-05). The precipitation values agree relatively well with ± 10 mm difference. Considering recent precipitation data might lead to more reasonable results in the future.

The LAP (LI-1), LND (LI-1), and LND (LI-2) values gradually increase with mean annual precipitation as shown in Fig. 7(c). The LND (LI-2) starts with higher value contrary to LAP (LI-1) and LND (LI-1). This is because of that the LI-2 contains many landslides in the southern part of the study area, where precipitation is low (see Figs. 2 and 13).

3.5 Correlations with Aftershock Parameters

High landslide density is witnessed near the epicenters of two aftershocks (with magnitudes of 6.7 and 7.3 occurred on April 26, 2015 and May 12, 2015, respectively) as shown in Fig. 2. The PGA maps and locations of epicenters for these two aftershocks were obtained from USGS (https://earthquake.usgs.gov/data/shakemap/) in vector format. The PGA maps were reclassified in the same bin size as that for the **M**7.8 main shock earthquake (i.e., 0.04 g), and the epicenter was buffered with 5-km bands.

The LAP (LI-1), LND (LI-1) and LND (LI-2) for PGA for the **M**7.3 aftershock are shown in Fig. 8(a). The LAP (LI-1) increases monotonically with an increase in PGA values indicating a strong correlation between the PGA and the landslide occurrence. The LND (LI-1) and LND (LI-2) show a similar trend until a PGA of 0.24 g, after which they slide down to rise again at a PGA of 0.29 g. The PGA for the **M**6.7 aftershock and corresponding LAP (LI-1), LND (LI-1), LND (LI-2) distributions are shown in Fig. 8(b). The LAP (LI-1) generally increases with PGA. The LND (LI-1) generally increase with PGA for PGA $\leq$ 0.4 g. Both LNDs show a sudden increase at a PGA of 0.4 g.

Figures 8(c) and 8(d) show the LAP (LI-1), LND (LI-1), and LND (LI-2) in terms of distance to the epicenters of the **M**7.3 aftershock and the **M**6.7 aftershock, respectively. The LAPs and LNDs are generally increasing with decreasing distances to epicenters. It is worth noting that the trends for the LNDs are stronger than those for the LAPs.

4. Comparison of the Effects of Landslide Conditioning Factors

The cumulative percentage of area and area under the curve (AUC) are commonly used to evaluate the relative influence of parameters on the landslide occurrence. The first step to compute the cumulative percentage of area is to reclassify the landslide conditioning factors into a number of bins. The second step is to compute the landslide-affected areas and class areas for the classes. LNDs and LAPs are then computed for the classes. After sorting LNDs and LAPs in a descending order, the cumulative percentage of landslide-affected areas/landslide numbers and class areas are computed to form the cumulative curves. When the curve is closer to the top left corner of the plot, the influence of a factor on the landslide occurrence is stronger.

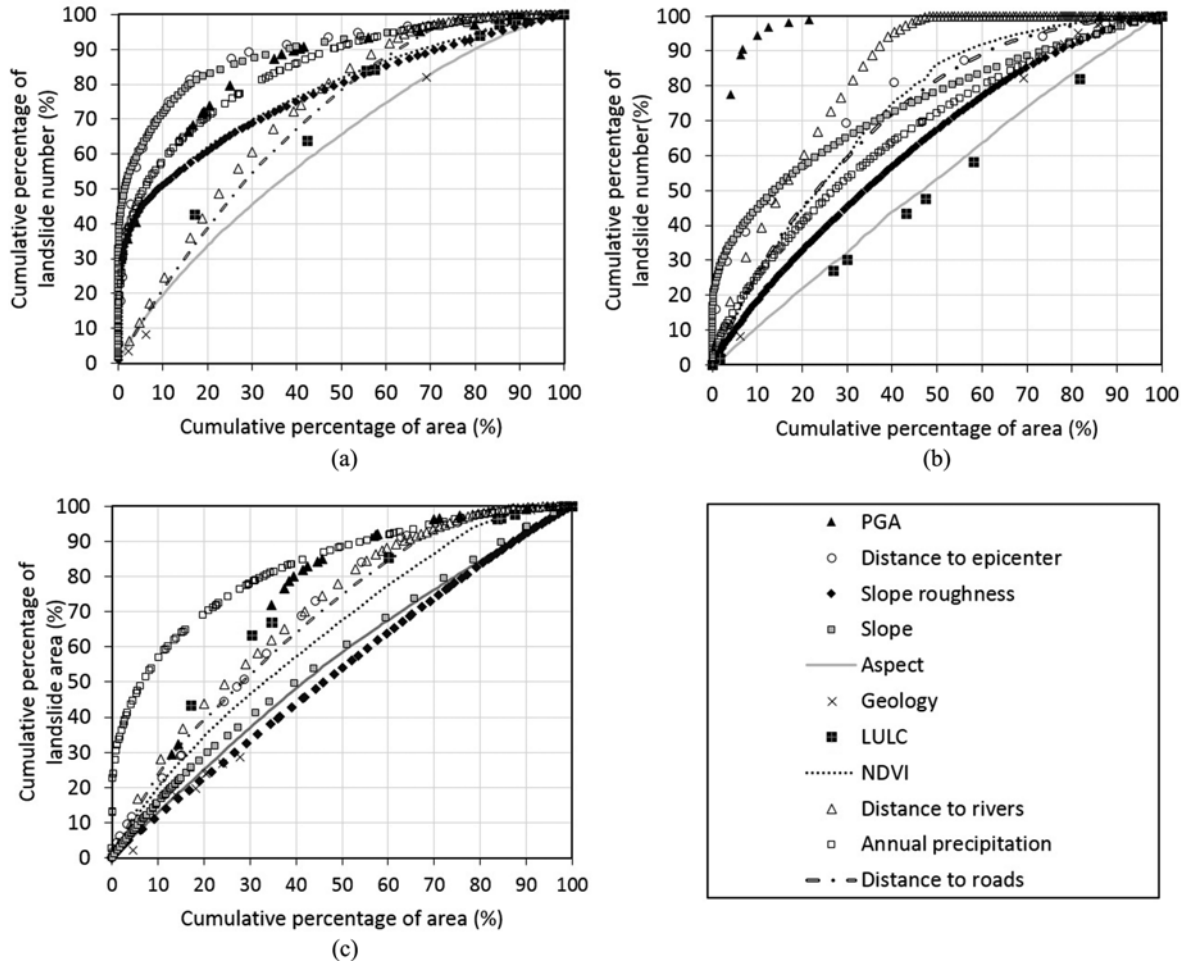

Fig. 9. Comparison of the Influence of Landslide Conditioning Factors on Landslide Occurrence: (a) Cumulative Curves – LND (LI-1), (b) Cumulative Curves – LND (LI-2), (c) Cumulative Curves – LAP (LI-1) (The curves for aftershock parameters are shown in Fig. 10.)

Table 2. Area under the Curve (AUC) for LAP (LI-1) and LNDs for Landslide Conditioning Factors

Conditioning factors	LND (LI-1)		LND (LI-2)		LAP (LI-1)	
	AUC	Rank	AUC	Rank	AUC	Rank
(a) PGA (**M**7.8)	84.05	5	79.08	5	73.43	4
(b) Epicentral distance	89.09	3	80.37	4	68.74	7
(c) Slope roughness	61.77	13	62.41	12	52.98	15
(d) Slope	84.42	4	78.23	6	57.11	12
(e) Aspect	61.63	14	60.8	13	55.29	13
(f) Geology	57.91	15	59.32	14	54.16	14
(g) LULC	67.92	12	48.4	15	70.32	5
(h) NDVI	76.62	7	76.85	7	63.56	11
(i) Distance to rivers	72.84	10	82.51	3	69.47	6
(j) Mean annual precipitation	78.02	6	66.41	11	81.15	3
(k) Distance to roads	69.49	11	71.64	9	68.1	8
(l) PGA (**M**7.3)	90.31	1	90.66	1	92.72	1
(m) PGA (**M**6.7)	89.9	2	87.32	2	82.4	2
(n) Epicentral distance (**M**7.3)	74.35	9	70.88	10	67.7	9
(o) Epicentral distance (**M**6.7)	75.93	8	73	8	67.16	10

Figure 9(a) shows cumulative percentages of landslide number for all of the considered factors for the **M**7.8 main shock earthquake event using the LI-1. In order to clearly summarize influence of the conditioning factors on the landslide occurrence, the areas under the curve (AUC) were computed from the cumulative percentage curves as shown in Table 2. The cumulative curve for the distance to the epicenter is closest to the top left corner, indicating the strongest influence of it on the landslide occurrence, compared to the other landslide conditioning factors. The influence is followed by slope > PGA of the **M**7.8 earthquake > mean annual precipitation > NDVI > distance to rivers > distance to roads > LULC > slope roughness > aspect > geology. This order does not consider the influence of aftershock parameters which are discussed in last paragraph of this section. It is worth noting that the slope is the most influencing factor among the vulnerability parameters, and the influence of it is greater than that of PGA of the main shock. The factors for the LI-2 were used to generate another set of cumulative curves as shown in Fig. 9(b). Distance to rivers shows the strongest correlation in influencing landslide occurrence compared to the rest of the parameters. The descending order of correlation among the factors is: distance to rivers > distance to epicenter of **M**7.8 earthquake > PGA of the **M**7.8 earthquake > slope > NDVI > distance to roads > mean annual precipitation > slope roughness > aspect > geology > LULC. The slope is the second most influencing factor among the vulnerability factors.

The cumulative percentages of landslide area for the LI-1 values are shown in Fig. 9(c). The correlation order is: mean annual precipitation > PGA of the **M**7.8 earthquake > LULC > distance to rivers > distance to epicenter > distance to roads > NDVI > slope > aspect > geology > slope roughness. The LAP (LI-1) curve trajectories are less curved compared to LND (LI-1) and LND (LI-2). The average AUC for the LAP (LI-1) is approximately 68.3, and is smaller than those for LND (LI-1) and LND (LI-2) (i.e., 75.6 and 72.5, respectively). This might be because of the LI-1 did not distinguish landslide debris piled at the bottom of slopes from landslide scarps, indicating that point data are more appropriate for landslide susceptibility mapping rather than polygon data.

The cumulative percentages of landslide number for the PGAs and epicentral distances of **M**7.8 main shock earthquake and two aftershock events using the LI-1 are compared as shown in Fig. 10(a). The PGA of aftershocks has a stronger correlation than the PGA of the main shock. This implies the possibility that the slopes became unstable when affected by the main shock ground motions and finally failed when hit by the aftershock ground motions. A similar comparison is carried out for using the LI-2 as shown in Fig. 10(b). The trend for the LI-2 agrees with that of the LI- 1. However, for the cumulative percentage of landslide area has a slight disagreement in the ranks as shown in Fig. 10(c). It turned out that the PGAs of the two aftershocks are most influencing factors among the hazard factors, based on all of the LND (LI-1), LND (LI-2), and LAP (LI-1).

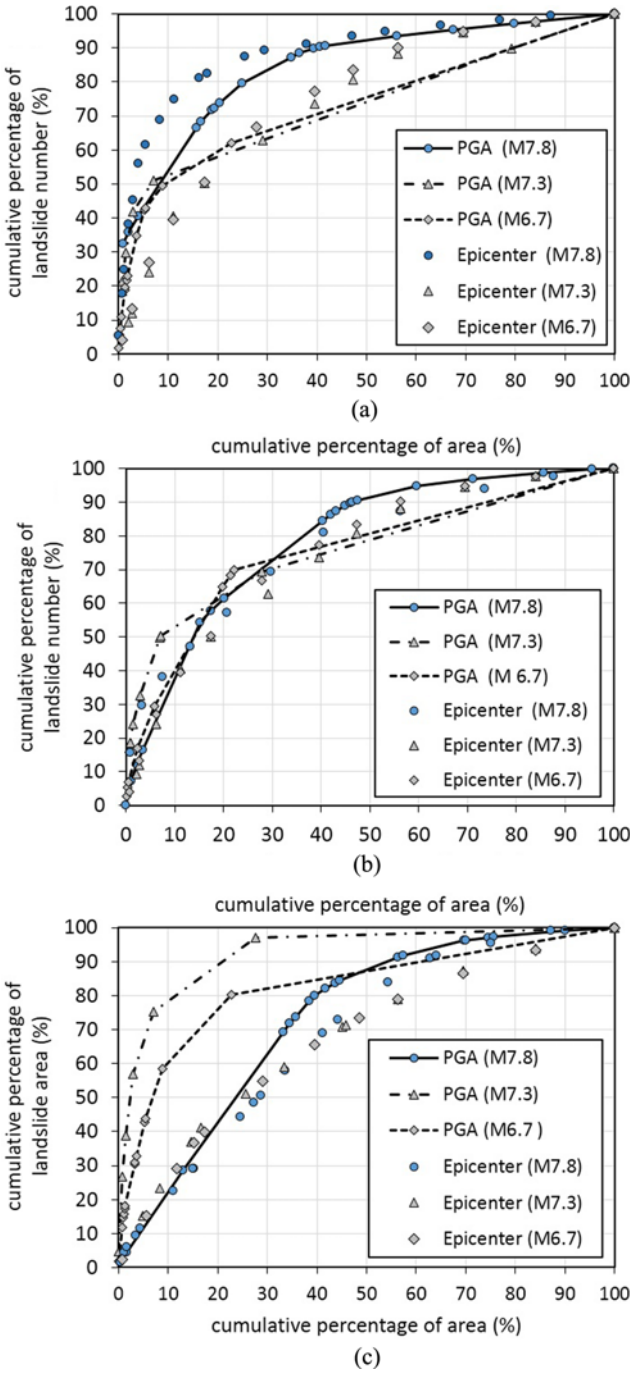

Fig. 10. Comparison of Influence on Landslide Occurrence on Aftershock PGA and Epicenters: (a) Cumulative Curves – LND (LI-1), (b) Cumulative Curves – LND (LI-2), (c) Cumulative Curves – LAP (LI-1)

5. Conclusions

Two landslide inventory sets (i.e., LI-1 and LI-2) were used to study the correlation of seismic landslide occurrences and the landslide conditioning factors such as slope, slope roughness, aspect, LULC, mean annual precipitation, distance to roads, rivers, PGA, and epicenters of the main shock earthquake and

aftershocks. The LI-1 is based on the sources available within the first few weeks of the earthquake and includes 1,352 landslide polygons. However, it does not differentiate landslide scarps and deposits, resulting in uncertainties with respect to exact landslide initiation locations. Therefore, the centroid points in the landslide polygons were identified as landslide initiation locations and used in the analyses in addition to the polygon data. The LI-2 was generated based on the data obtained several months after the earthquakes with extensive mapping tools and expert involvement and includes 4,000 point features. Therefore, it can be considered that the LI-2 is more complete. However, the LI-2 only has point features. The inclusion of polygons that differentiate scarps and deposits using high-resolution remote sensing elevation models like LiDAR (light detection and ranging) can help in the clear understanding of landslide correlations and lead to an accurate landslide susceptibility mapping in the future. This study considered both of the inventory data sets to take into account different characteristics the distinct inventory data sets.

Class area, LAP (using the LI-1), LND (using the LI-1), and LND (using the LI-2) plots were constructed for the aforementioned conditioning factors. The class area describes the distribution of the landslide conditioning factors in the study area, while the LAP and LND describe the influence of landslide conditioning factors in triggering landslides. The LAP and LND with respect to PGA of the main shock event show bimodality, indicating other factors have more influence on the landslide occurrence than the PGA. The LAP/LND generally increases with slope and slope roughness but does not show a trend with the aspect. In geological units, high LAP/LND values are noticed in Pc (Precambrian) and Q (Quaternary) and low in Mi (Mesozoic Intrusive), Ks (Cretaceous sedimentary rocks), and N (Neogene). The LAP/LND are high in needle leaved area (NL) and low in the agricultural valley. The NDVI value for the study area ranges between – 0.4 to + 0.5 and the LAP/LND increases with NDVI. The LAP/LND generally decreases with the distance to rivers and roads. The LAP/LND generally increase with precipitation, but the LI-2 contains numerous landslides observed in the low precipitation regions.

The cumulative percentage curves and areas under the curve (AUC) were used to examine the relative contributions of the conditional factors. The aftershock and main shock seismic parameters, slope angle, and distance to rivers have a strong influence in triggering a landslide. The LULC, geology, aspect, slope roughness, distance to road, and NDVI have relatively weak influence. The AUC values for the LAP (LI-1) are smaller than those for the LND (LI-1) and LND (LI-2), indicating that the point data better represent actual landslide locations rather than the polygon data.

Considering both main shock and aftershock parameters is meaningful because it provides relative contributions from main shock and aftershocks. The results showing that aftershock parameters are more strongly correlated with landslide occurrence than main shock parameters are quite interesting. The aftershock ground motion parameters have a stronger influence than those for the main shock event. This implies the possibility that the slopes became unstable when affected by the main shock ground motions and finally failed when hit by the aftershock ground motions.

Two limitations of this study are 1) it is possible that few landslide occurrences have been missed out by the reputed mapping agencies, and 2) the landslides generated by main shocks and aftershocks are not differentiated. These limitations can be overcome by the improved inventory data development in the future.

Acknowledgments

This research was supported by a grant (19SCIP-B146946-02) from Construction technology research program funded by Ministry of Land, Infrastructure and Transport of Korean government and the 2019 Research Fund (1.190047.01) of Ulsan National Institute of Science and Technology (UNIST). We would like to thank the two anonymous reviewers for their insightful comments.

ORCID

Byungmin Kim https://orcid.org/0000-0002-3290-7163

References

Ambraseys N, Bilham R (2000) A note on the Kangra Ms = 7.8 earthquake of 4 April 1905. *Current Science* 79:45-50, DOI: www.jstor.org/stable/24103320

Arabameri A, Pradhan B, Rezaei K (2019) Spatial prediction of gully erosion using ALOS PALSAR data and ensemble bivariate and data mining models. *Geosciences Journal* 23:669-686, DOI: 10.1007/s12303-018-0067-3

Bilham R, Ambraseys N (2005) Apparent Himalayan slip deficit from the summation of seismic moments for Himalayan earthquakes, 1500–2000. *Current Science* 88:6, DOI: www.jstor.org/stable/24110492

Bilham R, Bodin P, Jackson M (1995) Entertaining a great earthquake in western Nepal: Historick inactivity and geodetic tests for the present state of strain. *Journal of Nepal Geological Society* 11:73-78

Bilham R, Larson K, Freymueller J (1997) GPS measurements of present-day convergence across the Nepal Himalaya. *Nature* 386: 61, DOI: 10.1038/386061a0

Chen XL, Li CY, Wang MM, Li ZF (2011) The main factors causing the seismic landslide distribution difference on two sides of the faults - A case study of landslide distribution in Beichuan area. *Chinese Journal of Geophysics* 54:737-746, DOI: 10.3969/j.issn.0001-5733.2011.03.013

Chu L, Wang L-J, Jiang J, Liu X, Sawada K, Zhang J (2019) Comparison of landslide susceptibility maps using random forest and multivariate adaptive regression spline models in combination with catchment map units. *Geosciences Journal* 23(2):341-355, DOI: 10.1007/s12303-018-0038-8

Dahal RK, Hasegawa S (2008) Representative rainfall thresholds for landslides in the Nepal Himalaya. *Geomorphology* 100(3):429-443,

DOI: 10.1016/j.geomorph.2008.01.014

Dai FC, Xu C, Yao X, Xu L, Tu XB, Gong QM (2011) Spatial distribution of landslides triggered by the 2008 Ms 8.0 Wenchuan earthquake, China. *Journal of Asian Earth Sciences* 40(4):883-895, DOI: 10.1016/j.jseaes.2010.04.010

Gahalaut VK, Kundu B (2012) Possible influence of subducting ridges on the Himalayan arc and on the ruptures of great and major Himalayan earthquakes. *Gondwana Research* 21(4):1080-1088, DOI: 10.1016/j.gr.2011.07.021

Gerrard J, Gardner R (2002) Relationships between landsliding and land use in the Likhu Khola drainage basin, Middle Hills, Nepal. *Mountain Research and Development* 22(1):48-55, DOI: 10.1659/0276-4741(2002)022[0048:RBLALU]2.0.CO;2

Gupta HK (2015) The Mw 7.8 April 25, 2015 Nepal Earthquake (End of a long-term seismic quiescence?) *Journal of Geological Society of Inida* 85:641-646, DOI: 10.1007/s12594-015-0261-0

Hashash YMA, Tiwari B, Moss RES, Asimaki D, Clahan KB, Kieffer DS, Dreger DS, Macdonald A, Madugo CM, Mason HB, Pehlivan M, Rayamajhi D, Acharya I, Adhikari B (2015) Geotechnical field reconnaissance: Gorkha (Nepal) Earthquake of April 25, 2015 and related shaking sequence. Geotechnical Extreme Event Reconnaisance GEER Association Report No. GEER-040:1-250

Jade S, Bhatt BC, Yang Z, Bendick R, Gaur VK, Molnar P, Anand MB, Kumar D (2004) GPS measurements from the Ladakh Himalaya, India: Preliminary tests of plate-like or continuous deformation in Tibet. *GSA Bulletin* 116(11-12):1385-1391, DOI: 10.1130/B25357.1

Jibson RW, Crone AJ, Harp EL, Baum RL, Major JJ, Pullinger CR, Escobar CD, MartíNez M, Smith ME (2004) Landslides triggered by the 13 January and 13 February 2001 earthquakes in El Salvador. Natural Hazards in El Salvador. Natural Hazards in El Salvador 375:69-88, DOI: 10.1130/0-8137-2375-2.69

Kadirhodjaev A, Kadavi PR, Lee C-W, Lee S (2018) Analysis of the relationships between topographic factors and landslide occurrence and their application to landslide susceptibility mapping: A case study of Mingchukur, Uzbekistan. *Geosciences Journal* 22(6):1053-1067, DOI: 10.1007/s12303-018-0052-x

Kargel JS, Leonard GJ, Shugar DH, Haritashya UK, Bevington A, Fielding EJ, Fujita K, Geertsema M, Miles ES, Steiner J, Anderson E, Bajracharya S, Bawden GW, Breashears DF, Byers A, Collins B, Dhital MR, Donnellan A, Evans TL, Geai ML, Glasscoe MT, Green D, Gurung DR, Heijenk R, Hilborn A, Hudnut K, Huyck C, Immerzeel WW, Jiang Liming, Jibson R, Kääb A, Khanal NR, Kirschbaum D, Kraaijenbrink PDA, Lamsal D, Liu Shiyin, Lv Mingyang, Mckinney D, Nahirnick NK, Nan Zhuotong, Ojha S, Olsenholler J, Painter TH, Pleasants M, Kc P, Yuan Q, Raup BH, Regmi D, Rounce DR, Sakai A, Shangguan Donghui, Shea JM, Shrestha AB, Shukla A, Stumm D, Van Der Kooij M, Voss K, Wang Xin, Weihs B, Wolfe D, Wu Lizong, Yao Xiaojun, Yoder MR,Young N (2016) Geomorphic and geologic controls of geohazards induced by Nepal's 2015 Gorkha earthquake. *Science* 351(6269), DOI: 10.1126/science.aac8353

Keefer DK (1984) Landslides caused by earthquakes. *Geological Society of America Bulletin* 95:406-421, DOI: 10.1130/0016-7606(1984)95<406:LCBE>2.0.CO;2

Lee S, Dan NT (2005) Probabilistic landslide susceptibility mapping in the Lai Chau province of Vietnam: Focus on the relationship between tectonic fractures and landslides. *Environmental Geology* 48(6):778-787, DOI: 10.1007/s00254-005-0019-x

Lee S, Lee M-J, Lee S (2018) Spatial prediction of urban landslide susceptibility based on topographic factors using boosted trees. *Environmental Earth Sciences* 77(18):656, DOI: 10.1007/s12665-018-7778-7

Lee S, Pradhan B (2007) Landslide hazard mapping at Selangor, Malaysia using frequency ratio and logistic regression models. *Landslides* 4(1):33-41, DOI: 10.1007/s10346-006-0047-y

Liu F, Li J, Yang S (2015) Landslide erosion associated with the Wenchuan earthquake in the Minjiang River watershed: Implication for landscape evolution of the Longmen Shan, eastern Tibetan Plateau. *Natural Hazard* 76(3):1911-1926, DOI: 10.1007/s11069-014-1575-8

Mahalingam R, Olsen MJ, O'banion MS (2016) Evaluation of landslide susceptibility mapping techniques using lidar-derived conditioning factors (Oregon case study). *Geomatics, Natural Hazards and Risk* 7(6):1884-1907, DOI: 10.1080/19475705.2016.1172520

Murty TS, Rafiq M (1991) A tentative list of tsunamis in the marginal seas of the North Indian Ocean. *Natural Hazard* 4(1):81-83, DOI: 10.1007/bf00126560

Nandi A, Shakoor A (2010) A GIS-based landslide susceptibility evaluation using bivariate and multivariate statistical analyses. *Engineering Geology* 110(1):11-20, DOI: 10.1016/j.enggeo.2009.10.001

Pandey MR, Molnar P (1988) The distribution of Intensity of the bihar-Nepal earthquake of 15 January 1934 and bounds on the extent of the rupture zone. *Nepal Geological Society* 5:22-44

Ray RL, Jacobs JMJNH (2007) Relationships among remotely sensed soil moisture, precipitation and landslide events. *Natural Hazard* 43(2):211-222, DOI: 10.1007/s11069-006-9095-9

Richter CF, Allen CR, Nordquist JM (1958) The desert hot springs earthquakes and their tectonic environment. *Bulletin of the Seismological Society of America* 48(4):315-337

RodríGuez CE, Bommer JJ, Chandler RJ (1999) Earthquake-induced landslides: 1980-1997. *Soil Dynamics and Earthquake Engineering* 18(5):325-346, DOI: 10.1016/S0267-7261(99)00012-3

Sidle RC, Ziegler AD, Negishi JN, Nik AR, Siew R, Turkelboom F (2006) Erosion processes in steep terrain — Truths, myths, and uncertainties related to forest management in Southeast Asia. *Forest Ecology and Management* 224(1):199-225, DOI: 10.1016/j.foreco.2005.12.019

Thiery Y, Malet JP, Sterlacchini S, Puissant A, Maquaire O (2007) Landslide susceptibility assessment by bivariate methods at large scales: Application to a complex mountainous environment. *Geomorphology* 92(1):38-59, DOI: 10.1016/j.geomorph.2007.02.020

Wang L-J, Guo M, Sawada K, Lin J, Zhang J (2016a) A comparative study of landslide susceptibility maps using logistic regression, frequency ratio, decision tree, weights of evidence and artificial neural network. *Geosciences Journal* 20(1):117-136, DOI: 10.1007/s12303-015-0026-1

Wang Q, Li W, Xing M, Wu Y, Pei Y, Yang D, Bai H (2016b) Landslide susceptibility mapping at Gongliu county, China using artificial neural network and weight of evidence models. *Geosciences Journal* 20(5):705-718, DOI: 10.1007/s12303-016-0003-3

Wei X-L, Chen N-S, Cheng Q-G, He N, Deng M-F, Tanoli JIJJOMS (2014) Long-term activity of earthquake-induced landslides: A case study from Qionghai Lake Basin, Southwest of China. *Journal of Mountain Science* 11(3):607-624, DOI: 10.1007/s11629-013-2970-4

Xu C, Xu X, Dai F, Wu Z, He H, Shi F, Wu X, Xu S (2013) Application of an incomplete landslide inventory, logistic regression model and its validation for landslide susceptibility mapping related to the May 12, 2008 Wenchuan earthquake of China. *Natural Hazards* 68(2):883-900, DOI: 10.1007/s11069-013-0661-7

Yeats RS, Lillie RJ (1991) Contemporary tectonics of the Himalayan

frontal fault system: Folds, blind thrusts and the 1905 Kangra earthquake. *Journal of Structural Geology* 13(2):215-225, DOI: 10.1016/0191-8141(91)90068-T

Appendix

Figures 11 through 13 present spatial distributions of factors considered in this study.

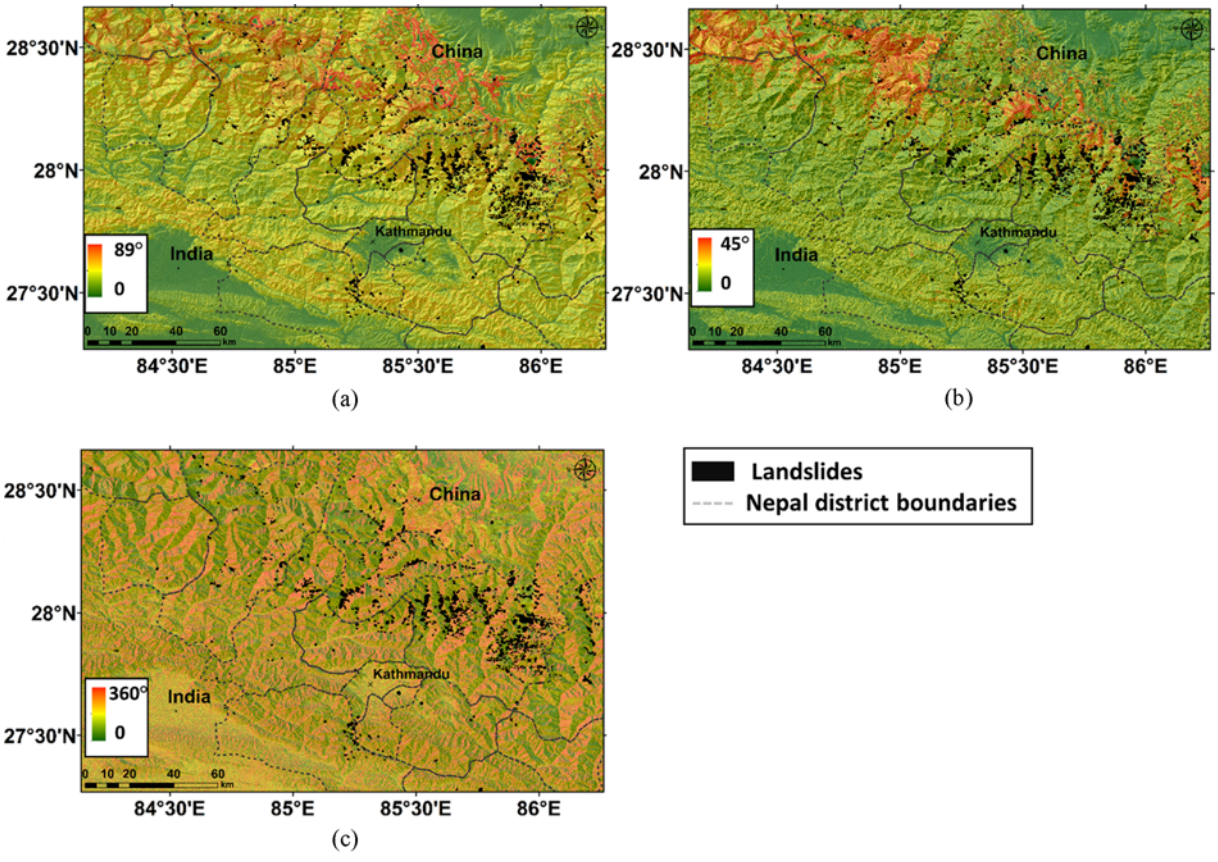

Fig. 11. Spatial Distributions of: (a) Slope Angle, (b) Slope Roughness, (c) Aspect with Landslide Inventory-1

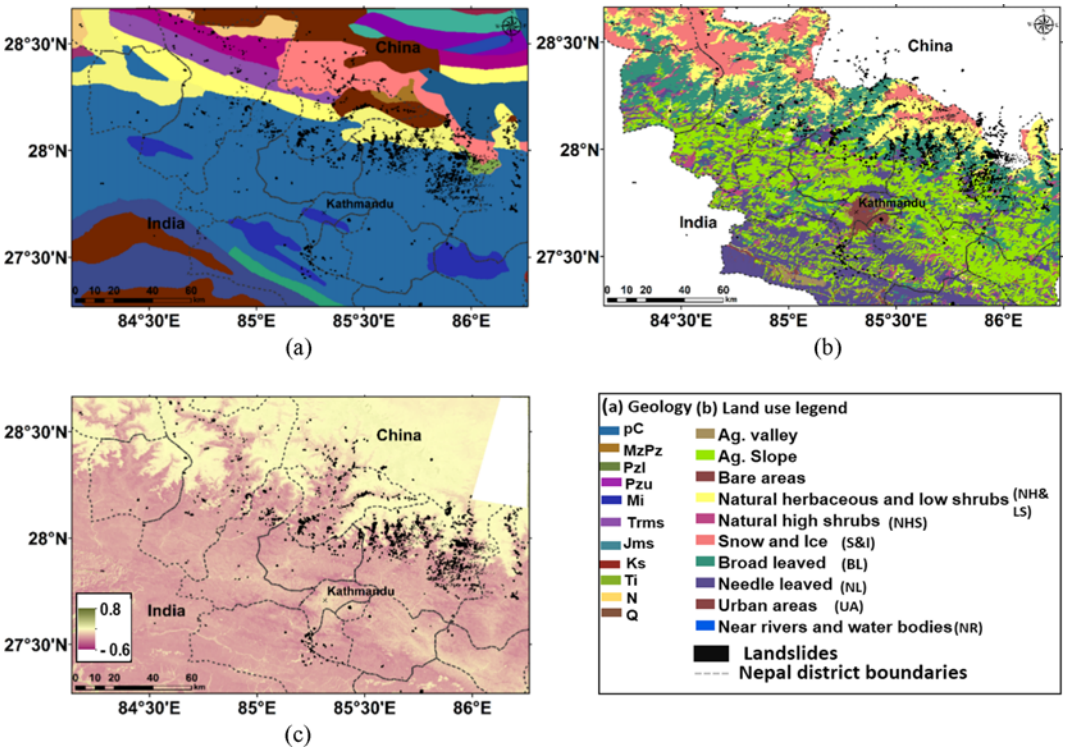

Fig. 12. Spatial Distributions of: (a) Geology, (b) Land Use, (c) NDVI with Landslide Inventory-1 (Acronyms for geology are Precambrian (pC); Mesozoic/Paleozoic (MzPz); Lower Paleozoic (Pzl); Upper Paleozoic (Pzu); Mesozoic Intrusive (Mi); Triassic metamorphic and sedimentary rocks (Trms); Jurrasic metamorphic and sedimentary rocks (Jms); Cretaceous sedimentary rocks (Ks); Tertiary igneous rocks (Ti);Neogene (N); Quaternary (Q))

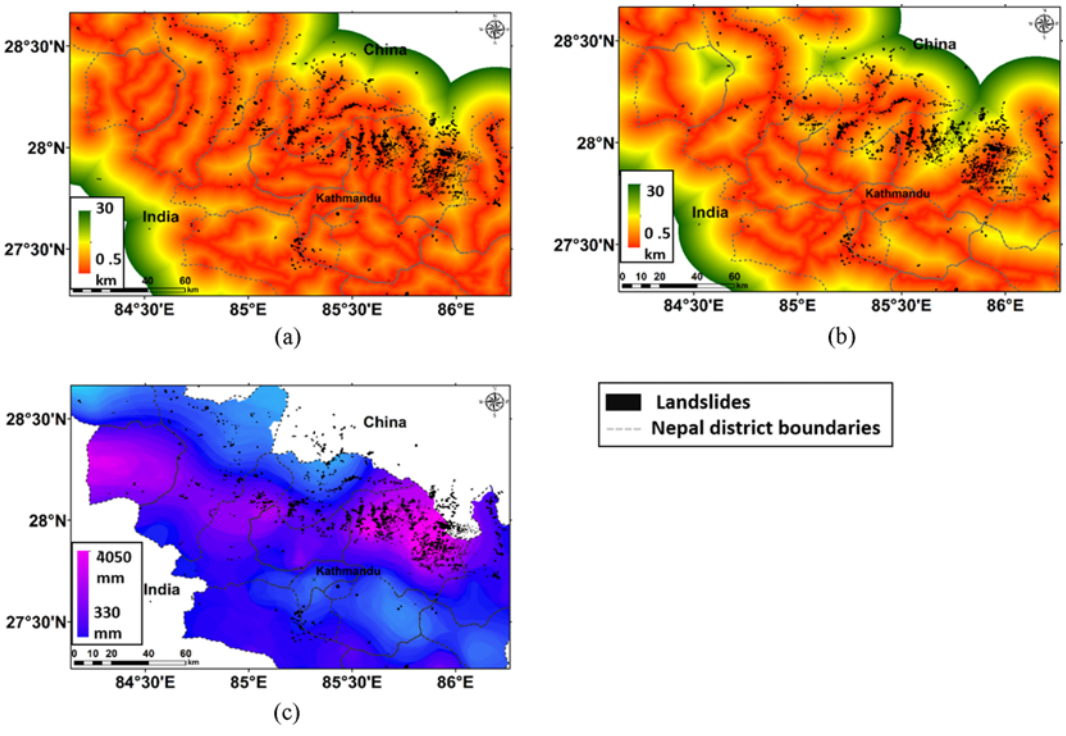

Fig. 13. Spatial Distributions of: (a) Rivers, (b) Roads, (c) Mean Annual Precipitation (1960 to 2000) with Landslide Inventory-1